Article

Kaolinite Thin Films Grown by Pulsed Laser Deposition and Matrix Assisted Pulsed Laser Evaporation

Luminita Nicoleta Dumitrescu [1], **Eusebiu-Rosini Ionita** [2,*], **Ruxandra Birjega** [1], **Andrada Lazea-Stoyanova** [2], **Maria-Daniela Ionita** [2], **George Epurescu** [1], **Ana-Maria Banici** [1], **Simona Brajnicov** [1], **Florin Andrei** [3] and **Andreea Matei** [1]

1   Lasers Department, National Institute for Lasers, Plasma and Radiation Physics, 409 Atomistilor Street, 077125 Magurele, Romania; nicoleta.dumitrescu@inflpr.ro (L.N.D.); ruxandra.birjega@inflpr.ro (R.B.); george.epurescu@inflpr.ro (G.E.); ana.niculescu@inflpr.ro (A.-M.B.); brajnicov.simona@inflpr.ro (S.B.); andreea.matei@inflpr.ro (A.M.)
2   Sources for Plasma and Applications Group, Low Temperature Plasma Laboratory, National Institute for Lasers, Plasma and Radiation Physics, 409 Atomistilor Street, 077125 Magurele, Romania; andrada@infim.ro (A.L.-S.); daniela.ionita@infim.ro (M.-D.I.)
3   Innovation Center in Photonics and Plasma for Advanced Materials and Technologies FOTOPLASMAT, National Institute for Lasers, Plasma and Radiation Physics, 409 Atomistilor Street, 077125 Magurele, Romania; florin.andrei@inflpr.ro
*   Correspondence: ionita.rosini@infim.ro; Tel.: +40-743109175

Abstract: In this work, thin films of lamellar clays were deposited by laser techniques (matrix assisted pulsed laser evaporation (MAPLE) and pulsed laser deposition (PLD)). The focus of this paper is the optimization of deposition parameters for the production of highly oriented crystalline films. The films were characterized by X-ray diffraction (XRD), X-ray photoelectron spectroscopy (XPS), atomic force microscopy (AFM), and scanning electron microscopy (SEM). Contact angle measurements were employed to identify the wetting properties of the deposited thin films. Hydrophobic to superhydrophilic films can be prepared by using different deposition techniques and deposition parameters. MAPLE led to superhydrophilic films with contact angles in the range $4°–8°$, depending on the microstructure and surface roughness at micro and nano scale. The 1064 nm PLD had a high deposition rate and produced a textured film while at $\lambda = 193$ nm an extremely thin and amorphous layer was depicted. Oriented kaolinite films were obtained by MAPLE even at 5 wt.% kaolinite in the target.

Keywords: laser processing; kaolinite; lamellar materials; thin films

1. Introduction

Lamellar clay materials are promising candidates as low-cost adsorbents with protein-binding capacities. Environmental industry uses clay minerals intensively for a variety of applications ranging from absorbance and storage of hazardous chemicals up to cleaning of polluted waters and sensing elements [1]. The main property of these lamellar materials is the adsorption capability, which is connected to the layer charge density, cationic charge capacity and swelling characteristic [2]. Kaolinite, being the most common clay mineral, is a lamellar material with the chemical formula ($Al_2O_3 \cdot 2SiO_2 \cdot 2H_2O$) and is used in several important fields as paper fabrication, pharmaceutical industry, cosmetics, or as adsorbents in water and wastewater treatment and many more [3]. These applications are based on the lamellar guest-host structure, which can adsorb a wide range of molecules, at the surface, at the edge of the lamellas or in the inter-lamellas [4]. Grafting reactions have been studied intensively in the last decades. For example, modified electrodes for electrochemical applications were synthesized in a two steps procedure, first grafting triethanolamine on the interlayer aluminol groups and then reacting with iodomethane for cyanide anions

detection [5]. Raw clays treated with hydrochloric acid and acetic acid were tested for adsorption of Cr (VI) and Fe (III) [6] and kaolin/polymer nanocomposite membranes were prepared for the removal of arsenic from aqueous solutions [7]. The detection of iodide in aqueous solution containing thiosulfate was reported onto a gold electrode modified by a thin film of kaolinite, obtained by grafting the ionic liquid (1-(2-hydroxyethyl)-4-(tert-butyl) pyridinium chloride) [8]. Wettability of hydrogen on kaolinite clay surfaces, in the presence of brine, was investigated for further use in hydrogen storage, with improved results as compared to illite or montmorillonite [9].Functionalized kaolinite hybrid materials with controlled interlayer distance were obtained by grafting trihydroxyethylmethylammonium iodide, 1-(2-hydroxyethyl)-3-methylimidazolium chloride and 1-benzyl-3-(2-hydroxyethyl) imidazolium chloride and were used as modified electrodes for electrochemical detection of different size ions of thiocyanate, sulphite and ferricyanide [10].

The most frequently used methods for kaolinite thin films deposition are solution cast technique [11], spin coating and electrochemical techniques [12]. O. G. Abdullah et al. [11] used solution cast technique for preparing composite material light films with different ratio of polyvinyl alcohol/kaolinite, and thicknesses ranging between 0.20 mm and 0.44 mm, aiming to study their optical properties. Kaolin light addition leads to a decrease of the optical energy gaps, while the Urbach energy tends to increase. N. Kouider et al. [12] describes the growth of porous and corrosion resistant films, via electrochemical coating method, using kaolin on stainless steel surfaces as modified electrodes suitable for methanol or ethanol fuel cells.

For the sensor industry, the aim is to obtain thin films with oriented structure and a high active area. Nowadays, the pulsed laser deposition systems are widely used in laboratories having the potential to deposit various oxide-based materials as metallic oxides films with a high degree of adhesion onto substrate [13,14]. The experimental set-up of the PLD system is simple and versatile with great development potential and compatibility for a wide variation of oxides and hydroxides. By using pulsed lasers and a vacuum chamber, a variety of stoichiometric oxide films can be grown in vacuum, reactive or inert background gas without the need for further processing [15]. Based on the vast applications (i.e., biotechnology, microelectronics, optoelectronics) that are relying on these oxides and hydroxides, an increasing research interest was observed regarding PLD technique in the processing of these materials. This laser-based method has many advantages, for example low processing duration for thin films of hundreds of nanometers and it is a non-polluting method, the laser being the energy source [16]. Moreover, PLD can produce films with excellent adhesion, due to the high energy of the species reaching the substrate [17,18]. These unique features of laser-based methods are suitable for the deposition/transfer of kaolinite thin films in sensor-based applications. Our work is focused on producing for the first time, via laser-based techniques, thin films of kaolinite with well controlled structure and aims to overcome the limitations of the classical deposition methods (cost, processing time, adhesion). In our experiments the laser methods bring the advantage of good thickness control. The ability of the laser methods to grow oriented and stoichiometric films of lamellar layered double hydroxides at room temperature has been previously demonstrated [19,20].

2. Materials and Methods

2.1. Materials

The following product was purchased and used without further purification: Kaolinite (KAOLINITE, NATURAL) FLUKA 03584-250G from (SIGMA-ALDRICH, CHEMIE GmbH, Riedstrt. 2 D-89555 Steinheim, Germany). The SEM images presented in Figure 1 highlight the lamellar structure of kaolinite powder. This clay powder was used in the preparation of PLD targets (by pressing with a hydraulic press with a pressure of ($\approx$20 MPa) applied to our kaolinite material) and MAPLE (by using an aqueous solution with 5 or 10 wt.% kaolinite in deionized water (as matrix)).

(**a**)

(**b**)
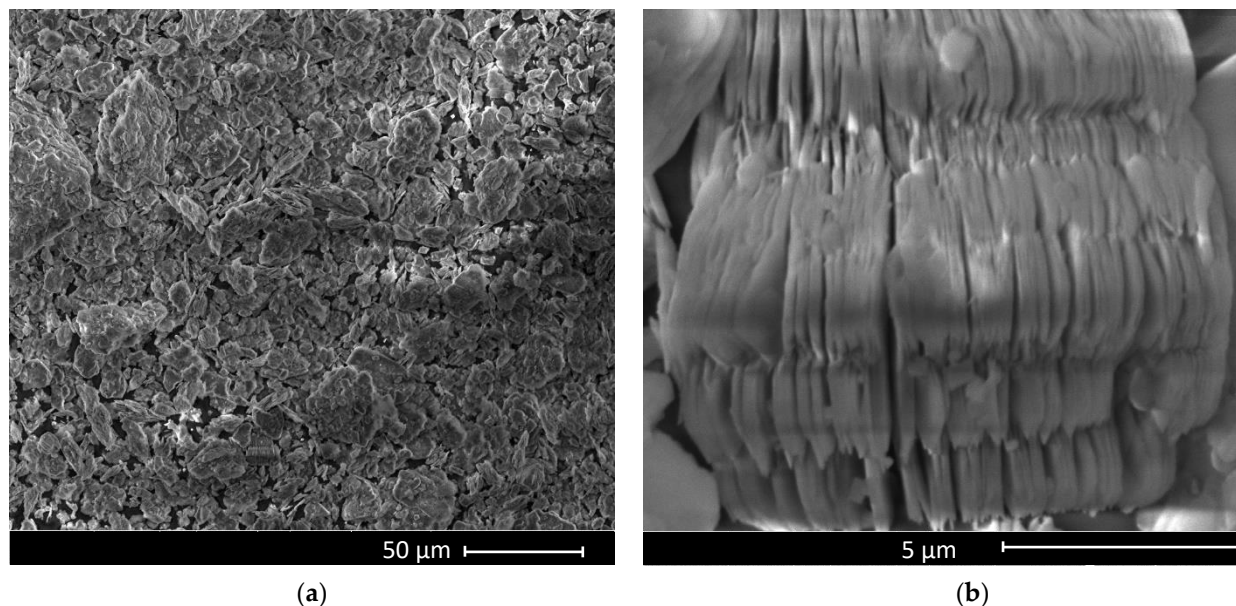
Figure 1. SEM images representing the topography of kaolinite powder with the magnifications of 1000× (**a**) and 20000× (**b**).

2.2. Lamellar Thin Films Deposition

Pulsed laser deposition (PLD) and matrix-assisted pulsed laser evaporation (MAPLE) experiments were performed starting from pressed kaolinite powder as targets for PLD technique, or from water-dispersed kaolinite solutions (5 or 10 wt.%) and then solidified/frozen by using liquid nitrogen, for the MAPLE method.

For PLD depositions, a Nd:YAG pulsed laser (Continuum Surelite II & Neocera workstation, Santa Clara, CA, USA) working in IR, VIS or UV and an ArF excimer laser at 193 nm were used to irradiate the target while for MAPLE, the fourth harmonic of the Nd:YAG pulsed laser working at 266 nm wavelength was chosen, based on our previous experiments [21–26]. The repetition rate was set at 10 Hz, the target and the substrate (Si <110>) were kept parallel at 4 cm distance, with the laser beam translated and the target rotated during depositions, for both PLD and MAPLE experiments. Kaolinite thin films were deposited by PLD method, as a result of 20.000–40.000 pulses at laser fluences ranging from 1 up to 5 J/cm^2, while for MAPLE technique, 72.000 pulses were used to irradiate the target with a laser fluence between 1 and 2 J/cm^2. The films deposition was made in vacuum conditions (1×10^{-5} mbar), with a small increase of the pressure during irradiation. For both PLD and MAPLE during experiments, the substrate (Si) was kept at room temperature (RT).

2.3. Characterization

X-ray diffraction (XRD) (PANalytical X'Pert MPD system, Almelo, The Netherlands) with a wavelength of 0.15418 nm was used for the crystalline structure investigation, for both powder material/target and deposited thin films. The HighScore software package (Version 4.0, PANalytical B.V., Almelo, The Netherlands, 2013) was used for the structural data analysis. X-ray photoelectron spectroscopy (XPS) survey spectra and high-resolution XPS scan spectra were acquired using an Escalab Xi+ system (Thermo Scientific, Waltham, MA, USA).

Thin films morphology and topography were analyzed by atomic force microscopy in ambient conditions, in non-contact mode-AFM XE-100 type from Park Systems, (Suwon, South Korea) and by scanning electron microscopy-SEM (FEI, model Inspect S50, Hillsboro, OR, USA) at an accelerating voltage of 10 kV.

In order to study the wettability of the surfaces as well as to determine the total free energy of the surface (SFE), contact angle measurements (WCA) were performed. For

this matter two types of liquids were used: water (double distilled) and methylene iodide (MI), water as polar liquid and MI as nonpolar liquid. Kaolinite thin film wettability was analyzed by sessile drop method using static contact angle measurements. The WCA measurements were made using an optical Contact Angle Tensiometer, CAM 101, from (KSV Instruments Ltd., Espoo, Finland), equipped with a CCD camera, an LED source, stands for substrate and a standard syringe from Hamilton (1000 μL). These wetting experiments were performed in the atmospheric environment at room temperature (RT) by placing the liquid droplet with the volume of 2 μL on the investigated surface. To calculate the total surface free energy (SFE) of the solids the Owens, Wendt, Rabel, and Kaelble (OWRK) [27,28] method was used. The solvents used in this SFE study for wetting experiments were: bidistilled water and methylene iodide (MI). The values for these solvents in terms of their dispersive and polar components are given in Table 1. These values used in the calculation of SFE are taken from the database of the device used to measure the contact angle.

Table 1. Total surface energy, dispersive and polar components for the solvents.

Solvent	Total Surface Energy [mN/m]	Dispersive Component [mN/m]	Polar Component [mN/m]
Bidistilled water	72.80	21.80	51.00
Methylene iodide	50.80	50.80	0.00

The DRIFT spectra of as deposited PLD films were collected using a JASCO (Tokyo, Japan) FT/IR-4700 spectrometer with a diffuse reflectance accessory (PIKE). The Si(001) substrate spectrum was extracted from the acquired spectra of the films.

3. Results and Discussion

Taking into account the profilometric measurements, it was observed that kaolinite thin films deposited as a result of target irradiation with 40.000 pulses for PLD and 72.000 pulses for MAPLE have thicknesses between tens of nanometers and a few microns, depending on the laser wavelength used for experiments. This leads to high deposition rates for PLD experiments, excepting 193 nm deposition and, considerably lower rates for MAPLE depositions. The comparison between deposition rate of kaolinite thin films using PLD and MAPLE methods is presented in Figure 2.
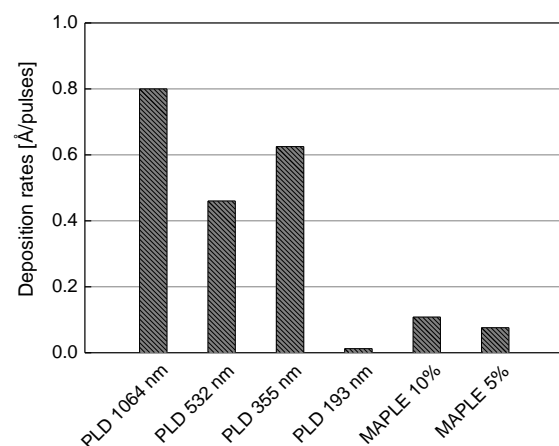
Figure 2. Kaolinite thin films deposition rates. Comparison between deposition methods: PLD and MAPLE.

The commercial powder from Fluka contains as dominant phase anorthic kaolinite-1A $Al_2 Si_2O_5(OH)_4$ (ICDD card 00-058-2028) and traces of monoclinic-$(SiO_2)_x$ (ICDD card 00-042-005). The same kaolinite 1A phase is found in the targets. The particular preparation

of the PLD target, by pressing, induced increased intensities of the (00*l*) reflections marking a preferred orientation of the layers along the *c*-axis (Figure 3a) The MAPLE target prepared by dispersing the kaolinite powder in water which is then dried in ambient atmosphere, exhibits also a preferred orientation along the *c*-axis due to the restacking of the layers in the aqueous solution (Figure 3b).
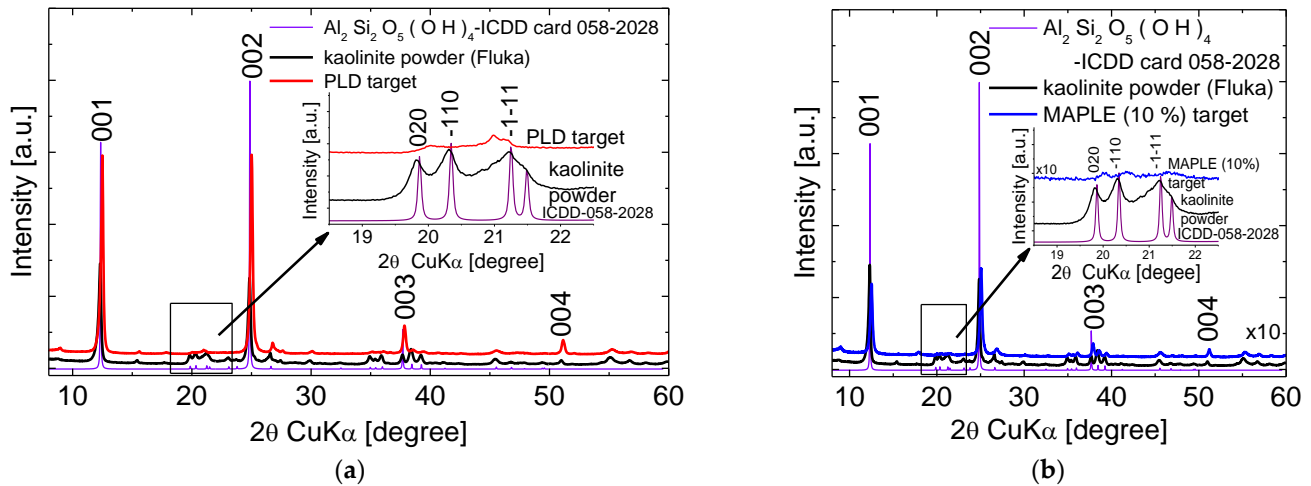
Figure 3. XRD patterns of the kaolinite commercial powder, (**a**) PLD target and (**b**) MAPLE target.

There is a large number of studies on the structure and proper definition of order and disorder in clays crystal structures [29]. The term of crystallinity is to be rather avoided in connection with clays and other parameters were introduced to describe the variety of order or disorder forms occurring in phyllosilicates [30]. We calculated two of such order-disorder indexes: the Hinckley index (HI), the most widely used, allowing a semi-quantitative evaluation of the degree of order-disorder of the kaolinite lattice, which was proposed in 1963 [31] and the Aparacio-Galan-Ferrel index (AGFI) proposed in 2006 [32]. In both cases, the indexes are determined by using reflections in the range 19° to 23° 2θ, considered to be sensitive to the structural defects as random and interlayer displacements. The HI includes the background in the calculation while, AGFI only the peaks intensities, which allows a higher degree of confidence. Values of HI < 0.5 and AGFI < 0.90 designates a disordered kaolinite while HI > 1.5 and AGFI >1.6 [29,30] characterizes an ordered kaolinite. FWHM-001 (F1) and FWHM-002 (F2) indexes determined as the width at half height of the basal reflections of kaolinite, (001) and (002), are the only one derived from oriented aggregates. Values (in degree) range from >0.4 (disordered) to <0.3 (ordered) [29]. The crystallite size D_{001} obtained from FWHM-001 through the Scherrer formula describes the thickness of coherent diffraction domain along the *c*-axis, which is the stacking axis of platy phyllosilicate layers. Awad et al. [33] found correlations between the crystallite size D_{001} of 28 kaolinite samples and their HI order-disordered index.

Table 2 presents the structural data and the above-described indexes for the commercial powder and the prepared targets. The d_{001} basal spacing calculated via the Bragg equation was also included. The targets preserved almost the same crystallographic parameters, namely the reduced unit cell parameters, hence their unit cell volume, as the commercial powder. The data shows that the commercial powder according to its HI, AGFI, F1 and F2 indexes is a low-defect kaolinite. Its crystallographic phase composition with very low amount of impurities and its high purity chemical composition, as the XPS data presented later, explain this result. The PLD target shows an increase of all the calculated order-disorder indexes. A. La Iglesia reported that very high static pressure induced disorder in kaolinites such as fractures, deformation and rolling of the layers [34,35]. The pressure of ≈ 20 MPa for the manufacture of the target/pellet used in the PLD experiments is 3 orders of magnitude less as those reported by La Iglesia. Actually, at this low-pressure value an increase of the coherence stacking layers distance occurs. The MAPLE target

presents a very slight decrease of the D_{001} size value and of the AGFI index as a result of the dissolution in water and the presence between the kaolinite layers of a larger number of polar hydroxyl groups.

Table 2. Structural data of the commercial powder and the targets obtained from XRD analysis.

Sample	Reduced Unit Cell Parameters							d_{001} (Å)	HI	AGFI	F1 (deg)	F2 (deg)	D_{001} (nm)
	a (Å)	b (Å)	c (Å)	α (°)	β (°)	γ (°)	Vol(Å^3)						
ICDD card 00-058-2028	5.156	7.409	8.950	88.18	89.81	75.34	330.59	7.1697					
powder	5.14(8)	7.40(9)	8.95(8)	88.0514(3)	89.91(2)	74.94(2)	328.67	7.214	1.14	1.53	0.27	0.23	33.7
PLD target	5.15(7)	7.38(6)	8.94(9)	88.0055(3)	89.62(2)	74.91(2)	328.14	7.102	1.68	1.63	0.24	0.21	37.4
MAPLE (10%) target	5.16(8)	7.36(7)	8.9(1)	88.9991(3)	89.61(2)	75.09(1)	327.80	7.081	1.25	1.04	0.30	0.27	31.0

There is a linear relationship between the overall order-disorder index AGFI and the size of the coherent diffraction domain perpendicular to the (001) plane, D_{001}. In conclusion the XRD analysis evidenced that the targets preparation procedures preserved all the intimate structural features of the commercial powder used for their preparation.

The XPS investigation employed to identify the chemical composition of lead to a ratio Al/Si of 0.82 (Table 3). The larger proportion of Si is consistent with the XRD observation of a small amount of SiO_2.

Table 3. Atomic composition for kaolinite powder.

Element	Atomic Ratio %
O1s	59.88
Si2p	19.15
Al2p	15.72
C1s	5.25

The PLD films show reflections except for the λ = 193 nm (Figure 4a and Table 4). No (hkl) with $h \neq 0$ and $k \neq 0$ is observable. For λ = 1064 nm all the four (00*l*) peaks are visible, and the intensities are high which turns this wavelength as the most effective one. The F1 and F2 values are <0.3° indicative of ordered kaolinite. In addition, the coherent domain size values characterizing the extension of the staking of layers, D_{001}, are slightly larger for the 1064 nm and 532 nm than the corresponding value for PLD target, indicative of highly oriented films. The d_{001} basal spacing values are similar to their corresponding PLD target, with a slight increment for the 1064 nm film, marking slight larger interlayer distance.

Table 4. Structural data of the films deposited via PLD and MAPLE.

Films	d_{001} (Å)	F1(deg)	F2(deg)	D_{001} (nm)
MAPLE 5%	7.014	0.274	0.247	33.8
MAPLE 10%	7.126	0.213	0.210	39.2
PLD 1064 nm	7.172	0.217	0.212	38.6
PLD 532 nm	7.005	0.197	0.184	42.4
PLD355 nm	7.127	0.243	0.172	34.4
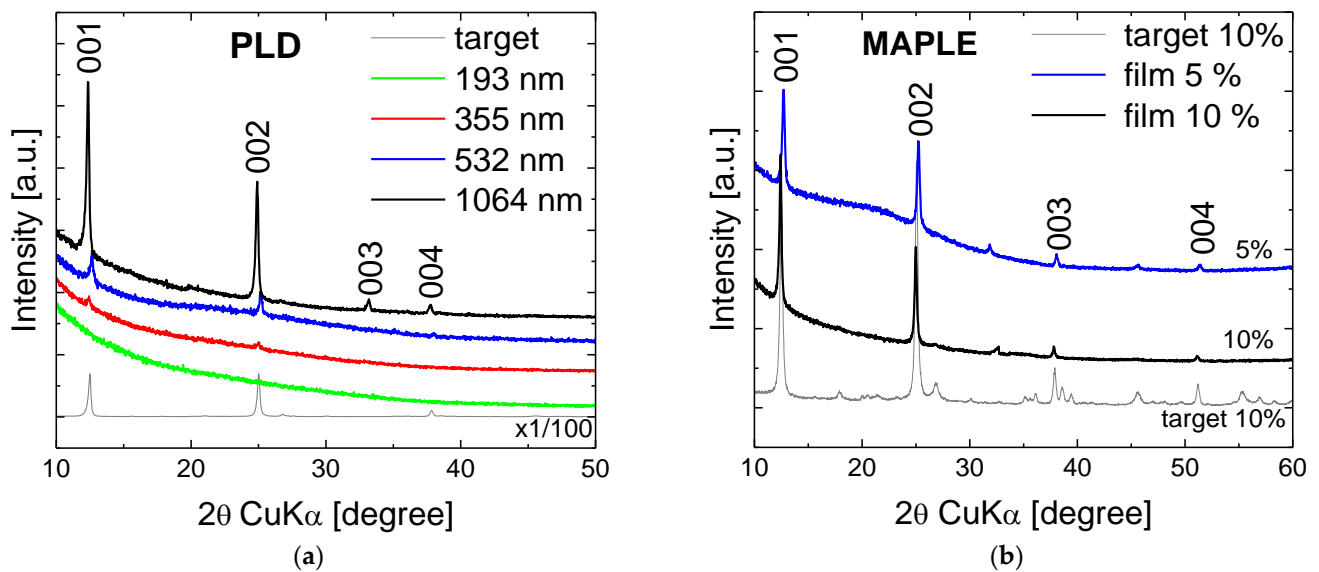
Figure 4. XRD patterns of the films deposited by PLD (**a**) and MAPLE (**b**) and their corresponding targets.

In the XRD patterns of MAPLE films (Figure 4b and Table 4) all the four (00*l*) reflections are clearly visible even for the film originating for the target with a lower concentration of 5%. The F1 and F2 indexes are also <0.3° with coherent domain sizes characterizing ordered kaolinite samples. The d_{001} basal spacing values are consistent with d_{001} spacing of the MAPLE (10%) target.

In conclusion the transfer of kaolinite as films via laser techniques from properly prepared targets produced highly oriented and ordered films in particular for 1064 nm wavelength for PLD and 10% concentration for MAPLE.

Scanning electron microscopy (SEM) and atomic force microscopy (AFM) used to study the surface morphology and the topography of the samples show clay films with a compact appearance, completely covering the substrate, with three-dimensional clusters and high roughness, especially for higher wavelengths (532 nm, 1064 nm). The decrease in laser fluence leads to a decrease in film roughness and a change in surface microstructure appearance. At 193 nm wavelength, the film surface is structured, dense, presenting grains in the range of tens of nanometers.

Figure 5 displays the SEM, whereas Figure 6 shows AFM images and the RMS roughness depending on the wavelength used for the experiments, correlated with the film thickness (Figure 7).

Samples elemental composition as analyzed by XPS is presented in Table 5 and Figure 8 it displays the presence of Si, Al and O, with similar composition found in the starting material, and ratio Al/Si smaller than 1, for most of the samples. The 193 nm PLD deposition is accompanied by Si leaching, consistent with the XRD measurements, supporting the decomposition of kaolinite structure.

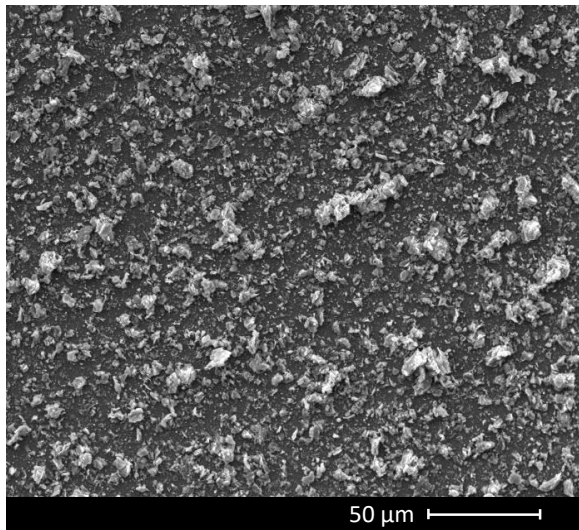**Table 5.** Films atomic composition and Al/Si ratio.

Atomic %	MAPLE 5%	MAPLE 10%	PLD 1064 nm	PLD 532 nm	PLD 335 nm	PLD 193 nm
O1s	66.22	65.33	62.79	60.92	62.63	63.06
Si2p	20.73	17.95	22.97	20.69	20.51	17.80
Al2p	13.05	16.71	14.24	18.39	16.85	19.13
Al/Si	0.63	0.93	0.62	0.88	0.82	1.07
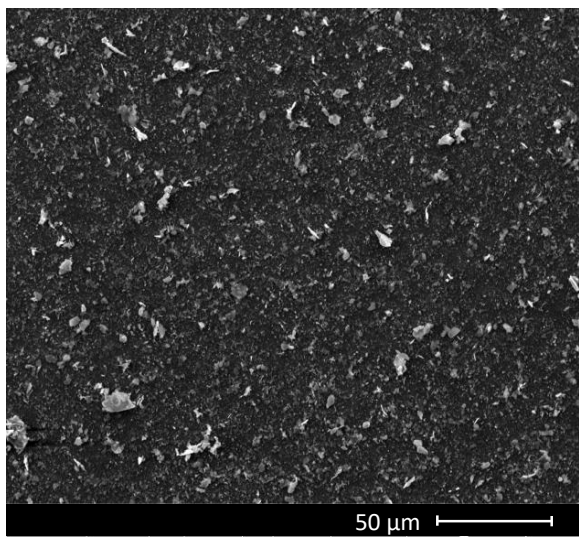
(**a**)
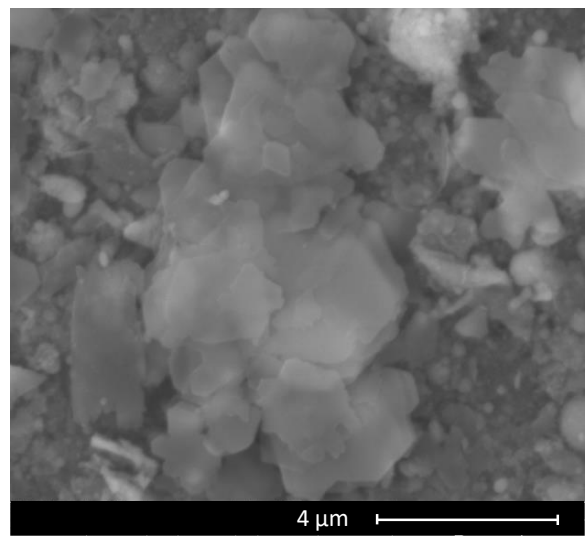
(**b**)

(**c**)

(**d**)

(**e**)

(**f**)

Figure 5. *Cont.*

(**g**)

(**h**)

(**i**)

(**j**)
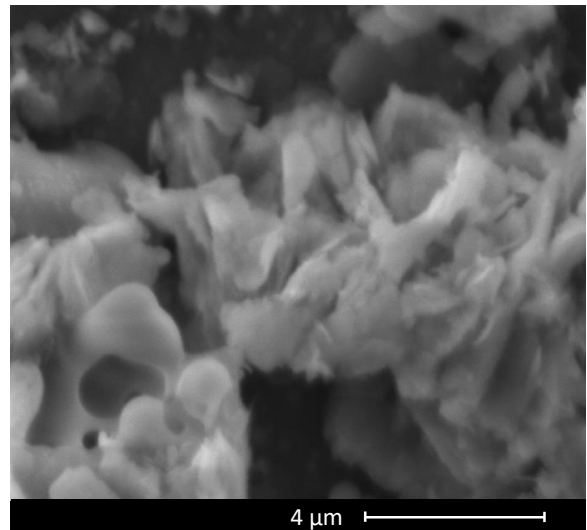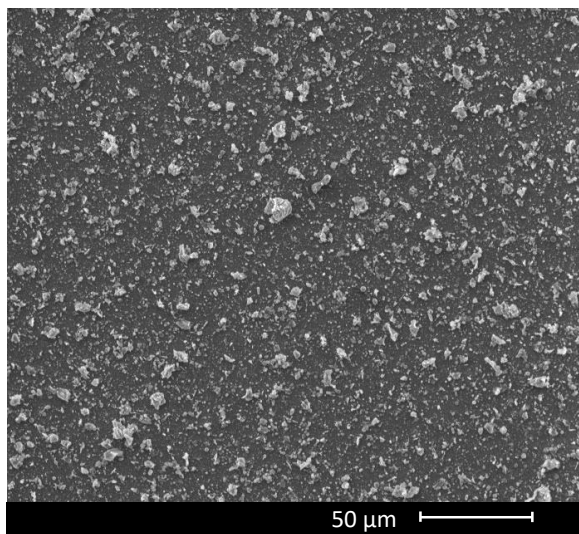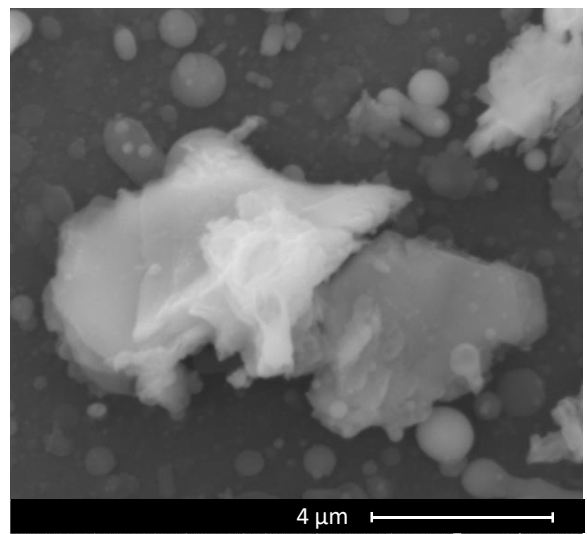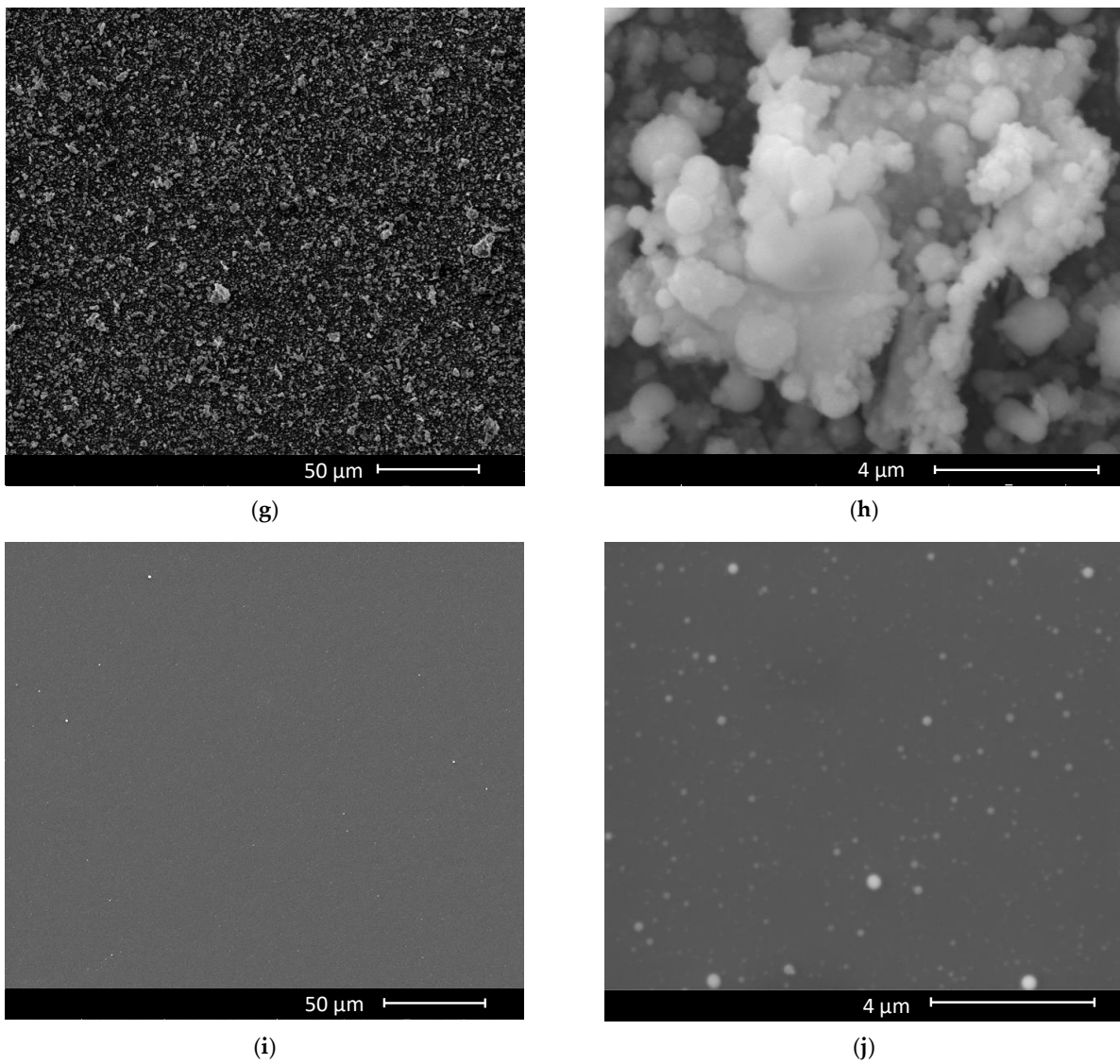
Figure 5. Grown films SEM images of MAPLE (**a**,**b**), PLD 1064 (**c**,**d**) and PLD 532 nm (**e**,**f**).Grown films SEM images of PLD 355 nm (**g**,**h**) and PLD 193 nm (**i**,**j**).

Figure 6. *Cont*.

PLD 1064 nm, 857 nm RMS

PLD 532 nm, 493 nm RMS

PLD 355 nm, 497 nm RMS

PLD 193 nm, 22 nm RMS
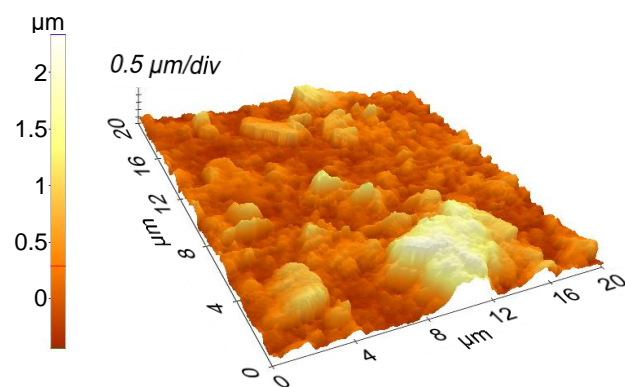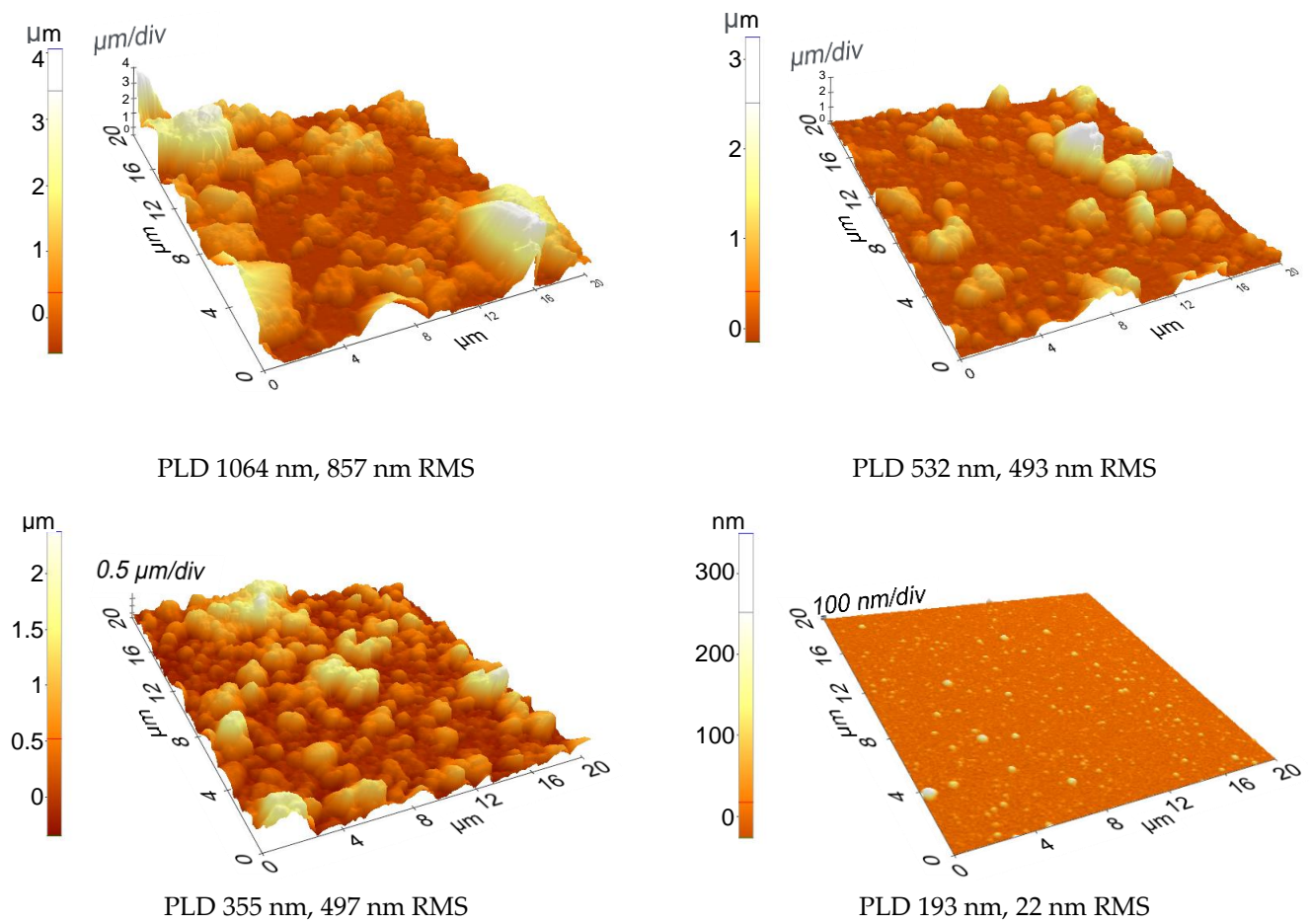
Figure 6. AFM image of films deposited by MAPLE; RMS roughness is 486 nm. AFM images and RMS roughness of films deposited by PLD.
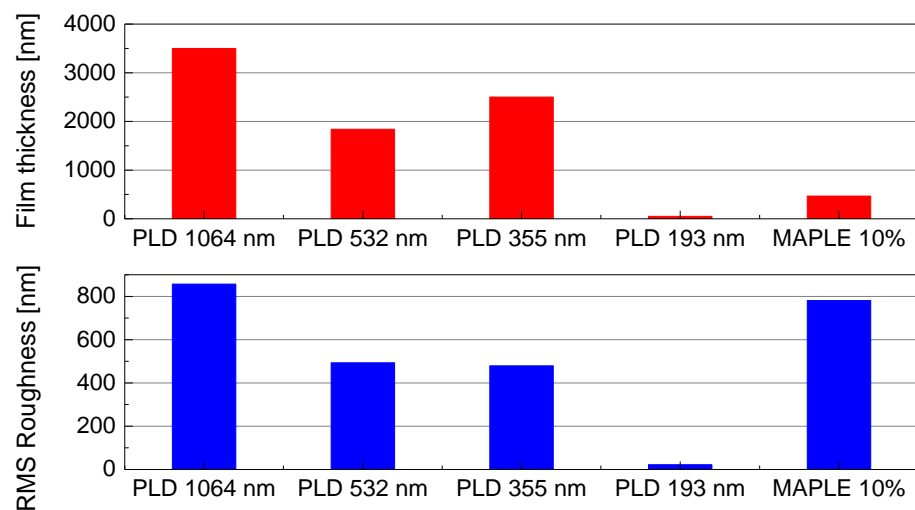
Figure 7. RMS roughness and thickness of films deposited by MAPLE and PLD.
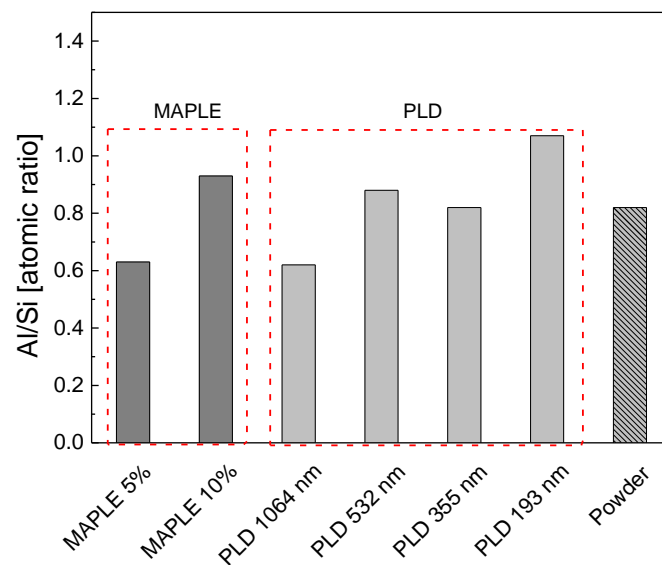
Figure 8. Al/Si atomic ratio for films deposited by MAPLE and PLD, as resulted from XPS survey.

In Figure 9a are shown water contact angle measurements (WCA) for kaolinite films obtained by PLD and MAPLE.

Figure 9. Contact angle (**a**) and surface energy components (**b**) for films deposited by MAPLE and PLD.

In general, the wettability of surfaces and implicitly the measurement of the water contact angle depends on many factors. For instance, in the case for clay minerals, wettability of the surface and the water contact angle is more complicated and difficult to determine and can be affected by: experimental procedure, film deposition method, deposition parameters, surface roughness, humidity, temperature, heterogeneity of 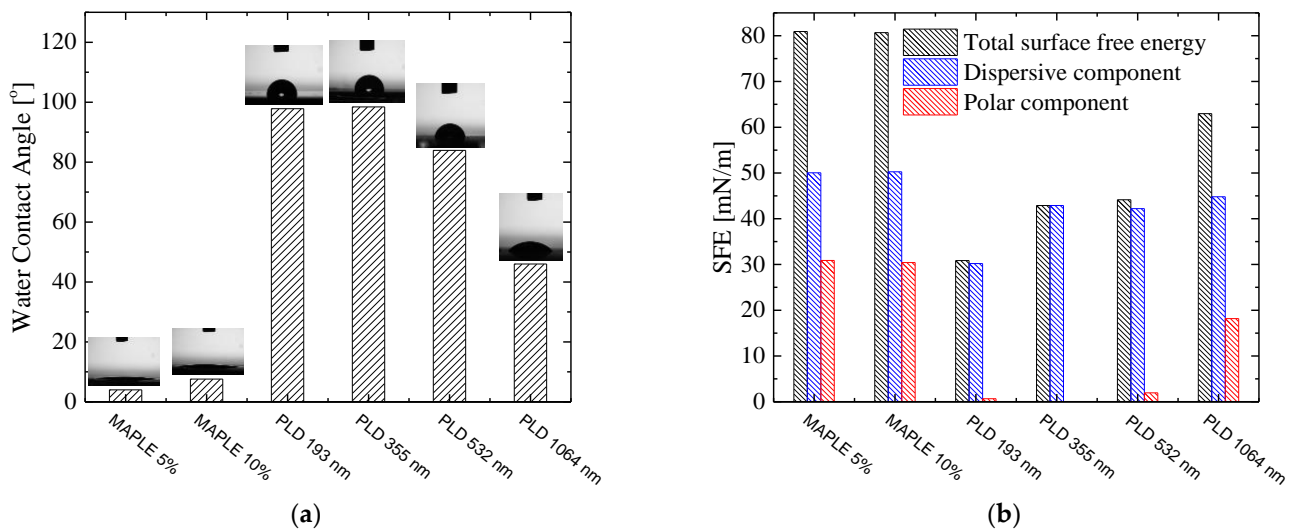surface, adsorption phenomena and particle size [36]. Some authors have reported that pure kaolinite has a hydrophilic or moderate hydrophilic character due to the hydroxyl groups on the surface [36–40] having a water contact angle value of 17–26°, respectively, 46.1° and 42°. In addition, in [36,41] the wetting characteristics of the silica tetrahedral face and alumina octahedral face of kaolinite was studied. The result of these study shows that the silica face of kaolinite has a modest level of hydrophobicity and the alumina face of kaolinite is hydrophilic.

In our case, similar values to those in the literature were found for water contact angle, namely 46° and was obtain for kaolinite film deposition by IR PLD techniques. As can be

seen from the graph, MAPLE leads to superhydrophilic films with contact angles in the range 4° and, respectively, 8°, depending on both the microstructure and surface roughness at micro and nano scale. Hydrophilic films with a water contact angle of about 46° can be obtained for IR PLD. In the case of PLD, at lower wavelengths it leads to water contact angles of around 98°.

For kaolinite films, surface energy and its components (polar and dispersive) were calculated by measuring the contact angle with water and methylene iodide. The surface energy and the contribution of polar and dispersive component are shown in the graph from Figure 9b. For the films deposited by MAPLE method, the polar components of surface energy are around 30 mN/m. The surface energy of the kaolinite films deposited by PLD was approximately 30.86 mN/m for wavelengths of 193 nm, 42.9 mN/m for 355 nm and 44.14 mN/m for 532 nm. The most important contribution is due to the dispersive components. For wavelength of 1064 nm, the surface energy of kaolinite film was 62.97 mN/m, polar component having the value of 18.16 mN/m.

From the results presented in this paper it is observed that the kaolinite films deposited by MAPLE technique have a higher affinity for water while the films deposited by PLD at lower wavelengths show a moderately water-repellent character. Kaolinite films deposited by IR PLD show moderate hydrophilicity.

These wetting behaviors are important and make them suitable for various applications in which these kaolinite films deposited by PLD and MAPLE can be used as active surfaces by functionalization or grafting with hydrophilic groups, as a support for use such as a sensor for protein detection, or as composite materials for temperature sensor and food packaging including.

The structural transformation and the reactivity of kaolinite involve dehydroxylation reactions [42]. In order to survey the effect of laser interaction on the molecular structure and in particular on the potential degradation of the hydroxyl groups in kaolinite we compared the DRIFT spectra of the PLD films deposited at 193 nm, 532 nm and 1064 nm, respectively. In the OH stretching region has four infrared active modes centered at 3695, 3670, 3650 and 3620 cm^{-1}. According to Farmer [43] the band at 3695 cm^{-1} is due to the in-phase inner surface hydroxyl stretching vibration, the two at 3670 and 3650 cm^{-1} to the out-of–phase vibrations of the inner surface hydroxyl and the band at 3620 cm^{-1} is the hydroxyl stretching vibration of the inner hydroxyl. The inner surface hydroxyls are also called outer hydroxyl groups and are situated in the outer upper, unshared plane, whereas the inner hydroxyl groups are located in the plane share with the apical oxygens of the tetrahedral sheet [44]. The resolution and the intensity of these bands depend on the defects in the kaolinite. However, the assignment of the hydroxyl stretching bands was and still is under constant review [45–47]. Thus, the information gained through such systems as *c*-oriented kaolinite films will add more knowledge on kaolinites and their behavior as functional material in prospects of future applications. The DRIFT spectra of the hydroxyl stretching region of the films deposited via PLD are presented in Figure 10. The spectrum of the film deposited at 193 nm was multiplied by 10 in order to be visualized. As in can be see the 3620 cm^{-1} peak corresponding to the inner hydroxyl groups are almost not shifted for the 532 nm and 1064 nm films (positioned at 3616 cm^{-1} for 532 nm film and at 3617cm^{-1} for 1064 nm film, respectively). The band is shifted to 3609 nm for 193 nm film signing structural alteration. Similarly, the in-phase inner-surface band at 3695 nm appears at 3693 cm^{-1} for 1064 cm^{-1} and at 3694 cm for 532 nm film while its position for the film deposited at 193 nm is seriously shifted towards 3730 cm^{-1}. The two bands corresponding the readily accessible out-of-phase outer hydroxyl groups are not so discernable and almost vanish for the 193 nm film, marking for this film a partial dexydroxylation accompanied by its structural deterioration. The spectra allure are similar to those of high-defect kaolinites [48], to kaolinites subject to mechanochemical activation via grinding which will decrease their crystallites sizes [48–50] or/and subjected to thermal treatments [42]. That means that all that the vibration of the inner surface hydroxyl groups are free and the OH groups are more readily accessible for exchange increasing their potentiality for functionalization. The

DRIFT data are consistent with the XRD results indicating the 1064 nm as the conducting to the most "crystalline" film while the film deposited at 193 nm is amorphous to XRD. For all these films deposited via PLD no band around 3555 cm^{-1} ascribed to water [51] is observable. The result is consistent with hydrophobicity of the PLD films of the as revealed by contact angle measurements. It is to be mentioned that the 1064 nm film exhibit a lower hydrophobicity probably due to its high roughness.
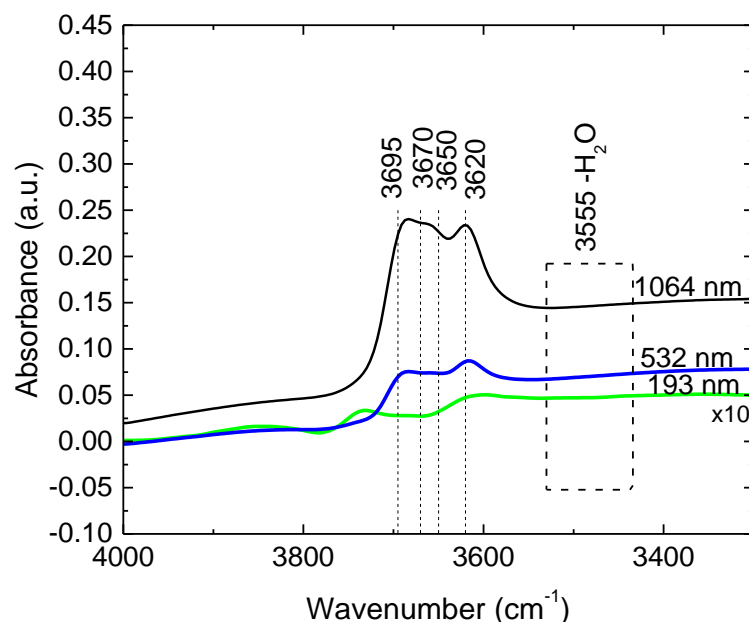
Figure 10. DRIFT spectra of the hydroxyl stretching region of the films deposited via PLD at 193 nm, 532 nm and 1064 nm.

4. Conclusions

We have successfully synthesized crystalline thin films of kaolinite using laser techniques, PLD and MAPLE, preserving the structure and chemical composition of the initial raw kaolinite. All the films are highly oriented along the *c*-axis. The 1064 nm wavelength for PLD secures the production of a thick and highly textured film while at λ = 193 nm an extremely thin and amorphous to XRD film is obtained. MAPLE proves to be effective for the deposition of highly oriented kaolinite films even at 5 wt.%. kaolinite in the target. It is a suitable technique for the deposition of clay films with pronounced hydrophilic character. To conclude our results, kaolinite thin films can be further used as active surfaces in electrochemical sensing.

Author Contributions: Conceptualization, A.M.; methodology, L.N.D.; validation, L.N.D., E.-R.I. and R.B.; formal analysis, R.B., A.-M.B., S.B. and F.A.; investigation, A.L.-S., M.-D.I. and G.E.; writing—original draft preparation, L.N.D., E.-R.I., A.M. and R.B.; writing—review and editing, A.M., R.B., E.-R.I., A.L.-S., L.N.D., G.E., M.-D.I., A.-M.B. and S.B.; visualization, E.-R.I.; supervision, A.M. and R.B.; project administration, G.E.; funding acquisition, A.M. All authors have read and agreed to the published version of the manuscript.

Data Availability Statement: Not applicable.

Conflicts of Interest: The authors declare no conflict of interest. The funders had no role in the design of the study; in the collection, analyses, or interpretation of data; in the writing of the manuscript, or in the decision to publish the results.

References

1. Ismadji, S.; Soetaredjo, F.E.; Ayucitra, A. Natural clay minerals as environmental cleaning agents. In *Clay Materials for Environmental Remediation*; Ismadji, S., Soetaredjo, F.E., Ayucitra, A., Eds.; Springer Briefs in Molecular Science; Springer International Publishing: Cham, Switzerland, 2015; pp. 5–37. ISBN 978-3-319-16712-1.

2. Bø Hunvik, K.W.; Loch, P.; Wallacher, D.; Kirch, A.; Cavalcanti, L.P.; Rieß, M.; Daab, M.; Josvanger, V.; Grätz, S.; Yokaichiya, F.; et al. CO_2 adsorption enhanced by tuning the layer charge in a clay mineral. *Langmuir* **2021**, *37*, 14491–14499. [CrossRef] [PubMed]

3. Leiviskä, T.; Gehör, S.; Eijärvi, E.; Sarpola, A.; Tanskanen, J. Characteristics and potential applications of coarse clay fractions from puolanka, Finland. *Open Eng.* **2012**, *2*, 239–247. [CrossRef]

4. Ghadiri, M.; Chrzanowski, W.; Rohanizadeh, R. Biomedical applications of cationic clay minerals. *RSC Adv.* **2015**, *5*, 29467–29481. [CrossRef]

5. Letaief, S.; Tonle, I.K.; Diaco, T.; Detellier, C. Nanohybrid materials from interlayer functionalization of kaolinite. Application to the electrochemical preconcentration of cyanide. *Appl. Clay Sci.* **2008**, *42*, 95–101. [CrossRef]

6. Dim, P.E.; Mustapha, L.S.; Termtanun, M.; Okafor, J.O. Adsorption of chromium (VI) and iron (III) ions onto acid-modified kaolinite: Isotherm, kinetics and thermodynamics studies. *Arab. J. Chem.* **2021**, *14*, 103064. [CrossRef]

7. Selvan, B.K.; Thiyagarajan, K.; Das, S.; Jaya, N.; Jabasingh, S.A.; Saravanan, P.; Rajasimman, M.; Vasseghian, Y. Synthesis and characterization of nano zerovalent iron-kaolin clay (NZVI-Kaol) composite polyethersulfone (PES) membrane for the efficacious As2O3 removal from potable water samples. *Chemosphere* **2022**, *288*, 132405. [CrossRef]

8. Nguelo, B.B.; Fomat, M.F.; Dedzo, G.K.; Ngameni, E. Catalytic detection of iodide at cationic kaolinite modified gold electrode in presence of thiosulfate. *Electroanalysis* **2020**, *32*, 1417–1425. [CrossRef]

9. Al-Yaseri, A.; Wolff-Boenisch, D.; Fauziah, C.A.; Iglauer, S. Hydrogen wettability of clays: Implications for underground hydrogen storage. *Int. J. Hydrog. Energy* **2021**, *46*, 34356–34361. [CrossRef]

10. Dedzo, G.K.; Letaief, S.; Detellier, C. Kaolinite–ionic liquid nanohybrid materials as electrochemical sensors for size-selective detection of anions. *J. Mater. Chem.* **2012**, *22*, 20593–20601. [CrossRef]

11. Abdullah, O. Effect of kaolin light concentration on optical characteristic of PVA films. *Asian Trans. Sci. Amp. Technol.* **2011**, *1*, 12–15.

12. Brooksby, P.A.; Downard, A.J. Electrochemical and atomic force microscopy study of carbon surface modification via diazonium reduction in aqueous and acetonitrile solutions. *Langmuir* **2004**, *20*, 5038–5045. [CrossRef] [PubMed]

13. Lackner, J.M.; Waldhauser, W.; Ebner, R.; Major, B.; Schöberl, T. pulsed laser deposition of titanium oxide coatings at room temperature—Structural, mechanical and tribological properties. *Surf. Coat. Technol.* **2004**, *180–181*, 585–590. [CrossRef]

14. Filipescu, M.; Papavlu, A.P.; Dinescu, M. *Functional Metal Oxide Thin Films Grown by Pulsed Laser Deposition*; IntechOpen: London, UK, 2016; ISBN 978-953-51-2446-7.

15. Cichetto, L.; Sergeenkov, S.; Diaz, J.C.C.A.; Longo, E.; Araújo-Moreira, F.M. Influence of substrate on structural and transport properties of LaNiO3 thin films prepared by pulsed laser deposition. *AIP Adv.* **2017**, *7*, 025005. [CrossRef]

16. Masood, K.B.; Kumar, P.; Malik, M.A.; Singh, J. A comprehensive tutorial on the pulsed laser deposition technique and developments in the fabrication of low dimensional systems and nanostructures. *Emergent Mater.* **2021**, *4*, 737–754. [CrossRef]

17. Liu, Z. 4.09—Laser applied coatings. In *Shreir's Corrosion*; Cottis, B., Graham, M., Lindsay, R., Lyon, S., Richardson, T., Scantlebury, D., Stott, H., Eds.; Elsevier: Oxford, UK, 2010; pp. 2622–2635. ISBN 978-0-444-52787-5.

18. Orava, J.; Kohoutek, T.; Wagner, T. 9—Deposition techniques for chalcogenide thin films. In *Chalcogenide Glasses*; Adam, J.-L., Zhang, X., Eds.; Woodhead Publishing: Cambridge, UK, 2014; pp. 265–309. ISBN 978-0-85709-345-5.

19. Birjega, R.; Matei, A.; Filipescu, M.; Stokker-Cheregi, F.; Luculescu, C.; Colceag, D.; Zavoianu, R.; Pavel, O.D.; Dinescu, M. The investigation of Ni–Al and Co–Al based layered double hydroxides and their derived mixed oxides thin films deposited by pulsed laser deposition. *Appl. Surf. Sci.* **2013**, *278*, 122–126. [CrossRef]

20. Birjega, R.; Matei, A.; Mitu, B.; Ionita, M.D.; Filipescu, M.; Stokker-Cheregi, F.; Luculescu, C.; Dinescu, M.; Zavoianu, R.; Pavel, O.D.; et al. Layered double hydroxides/polymer thin films grown by matrix assisted pulsed laser evaporation. *Thin Solid Film.* **2013**, *543*, 63–68. [CrossRef]

21. Vlad, A.; Birjega, R.; Matei, A.; Luculescu, C.; Mitu, B.; Dinescu, M.; Zavoianu, R.; Pavel, O.D. Retention of heavy metals on layered double hydroxides thin films deposited by pulsed laser deposition. *Appl. Surf. Sci.* **2014**, *302*, 99–104. [CrossRef]

22. Matei, A.; Birjega, R.; Nedelcea, A.; Vlad, A.; Colceag, D.; Ionita, M.D.; Luculescu, C.; Dinescu, M.; Zavoianu, R.; Pavel, O.D. Mg–Al layered double hydroxides (LDHs) and their derived mixed oxides grown by laser techniques. *Appl. Surf. Sci.* **2011**, *257*, 5308–5311. [CrossRef]

23. Matei, A.; Birjega, R.; Vlad, A.; Filipescu, M.; Nedelcea, A.; Luculescu, C.; Zavoianu, R.; Pavel, O.D.; Dinescu, M. Adsorption properties of Mg–Al layered double hydroxides thin films grown by laser based techniques. *Appl. Surf. Sci.* **2012**, *258*, 9466–9470. [CrossRef]

24. Matei, A.; Birjega, R.; Vlad, A.; Luculescu, C.; Epurescu, G.; Stokker-Cheregi, F.; Dinescu, M.; Zavoianu, R.; Pavel, O.D. Pulsed laser deposition of Mg–Al layered double hydroxide with ag nanoparticles. *Appl. Phys. A* **2013**, *110*, 841–846. [CrossRef]

25. Birjega, R.; Matei, A.; Marascu, V.; Vlad, A.; Ionita, M.D.; Dinescu, M.; Zăvoianu, R.; Corobea, M.C. Stearic acid/layered double hydroxides composite thin films deposited by combined laser techniques. *Molecules* **2020**, *25*, 4097. [CrossRef] [PubMed]

26. Baciu, D.D.; Matei, A.; Visan, T. Extraction procedure and cyclic voltammetry assay for detection of monosodium glutamate from different processed food sources. *Rev. Chim.* **2020**, *71*, 63–71. [CrossRef]

27. Owens, D.K.; Wendt, R.C. Estimation of the surface free energy of polymers. *J. Appl. Polym. Sci.* **1969**, *13*, 1741–1747. [CrossRef]

28. Kaelble, D.H. Dispersion-polar surface tension properties of organic solids. *J. Adhes.* **1970**, *2*, 66–81. [CrossRef]

29. Aparicio, P.; Galán, E. Mineralogical interference on kaolinite crystallinity index measurements. *Clays Clay Miner.* **1999**, *47*, 12–27. [CrossRef]

30. Guggenheim, S.; Adams, J.M.; Bain, D.C.; Bergaya, F.; Brigatti, M.F.; Drits, V.A.; Formoso, M.L.L.; Galán, E.; Kogure, T.; Stanjek, H. Summary of recommendations of nomenclature committees relevant to clay mineralogy: Report of the association internationale pour l'etude des argiles (AIPEA) nomenclature committee for 2006. *Clays Clay Miner.* **2006**, *54*, 761–772. [CrossRef]

31. Hinckley, D.N. Mineralogical and chemical variations in the kaolin deposits of the coastal plain of georgia and south carolina. *Am. Mineral.* **1965**, *50*, 1865–1883.

32. Aparicio, P.; Galán, E.; Ferrell, R.E. A new kaolinite order index based on XRD profile fitting. *Clay Miner.* **2006**, *41*, 811–817. [CrossRef]

33. Awad, M.E.; López-Galindo, A.; Sánchez-Espejo, R.; Sainz-Díaz, C.I.; El-Rahmany, M.M.; Viseras, C. Crystallite size as a function of kaolinite structural order-disorder and kaolin chemical variability: Sedimentological implication. *Appl. Clay Sci.* **2018**, *162*, 261–267. [CrossRef]

34. Iglesia, A.L. Pressure induced disorder in kaolinite. *Clay Miner.* **1993**, *28*, 311–319. [CrossRef]

35. La Iglesia, A.; Aznar, A.J. Crystallinity variations in kaolinite induced by grinding and pressure treatments. *J. Mater. Sci.* **1996**, *31*, 4671–4677. [CrossRef]

36. Yin, X.; Gupta, V.; Du, H.; Wang, X.; Miller, J.D. Surface charge and wetting characteristics of layered silicate minerals. *Adv. Colloid Interface Sci.* **2012**, *179–182*, 43–50. [CrossRef] [PubMed]

37. Jańczuk, B.; Chibowski, E.; Hajnos, M.; Białopiotrowicz, T.; Stawiński, J. Influence of exchangeable cations on the surface free energy of kaolinite as determined from contact angles. *Clays Clay Miner.* **1989**, *37*, 269–272. [CrossRef]

38. Shang, J.; Flury, M.; Harsh, J.B.; Zollars, R.L. Contact angles of aluminosilicate clays as affected by relative humidity and exchangeable cations. *Colloids Surf. Physicochem. Eng. Asp.* **2010**, *353*, 1–9. [CrossRef]

39. Günay, M.; Erdoğan, M.K.; Karakışla, M.; Saçak, M. Hydrophobic modification of kaolinite by coating with the conductive polythiophene and investigation of the usability as the environmental-based sensors. *Chem. Pap.* **2021**, *75*, 123–137. [CrossRef]

40. Wu, W. Baseline studies of the clay minerals society source clays: Colloid and surface phenomena. *Clays Clay Miner.* **2001**, *49*, 446–452. [CrossRef]

41. Liu, J.; Wang, X.; Lin, C.-L.; Miller, J.D. Significance of particle aggregation in the reverse flotation of kaolinite from bauxite ore. *Miner. Eng.* **2015**, *78*, 58–65. [CrossRef]

42. Drits, V.A.; Derkowski, A.; Sakharov, B.A.; Zviagina, B.B. Experimental evidence of the formation of intermediate phases during transition of kaolinite into metakaolinite. *Am. Mineral.* **2016**, *101*, 2331–2346. [CrossRef]

43. Farmer, V.C. Differing effects of particle size and shape in the infrared and raman spectra of kaolinite. *Clay Miner.* **1998**, *33*, 601–604. [CrossRef]

44. Frost, R.L.; Horváth, E.; Makó, É.; Kristóf, J.; Rédey, Á. Slow Transformation of mechanically dehydroxylated kaolinite to kaolinite—An aged mechanochemically activated formamide-intercalated kaolinite study. *Thermochim. Acta* **2003**, *408*, 103–113. [CrossRef]

45. Ledoux, R.L.; White, J.L. Infrared study of the OH groups in expanded kaolinite. *Science* **1964**, *143*, 244–246. [CrossRef] [PubMed]

46. Johansson, U.; Holmgren, A.; Forsling, W.; Frost, R. Isotopic exchange of kaolinite hydroxyl protons: A diffuse reflectance infrared fourier transform spectroscopy study. *Analyst* **1998**, *123*, 641–645. [CrossRef]

47. Han, Y.; Yan, Z.; Jin, L.; Liao, J.; Feng, G. In situ study on interactions between hydroxyl groups in kaolinite and re-adsorption water. *RSC Adv.* **2020**, *10*, 16949–16958. [CrossRef]

48. Frost, R.L.; Horváth, E.; Makó, É.; Kristóf, J. Modification of low- and high-defect kaolinite surfaces: Implications for kaolinite mineral processing. *J. Colloid Interface Sci.* **2004**, *270*, 337–346. [CrossRef] [PubMed]

49. Makó, É.; Frost, R.L.; Kristóf, J.; Horváth, E. The effect of quartz content on the mechanochemical activation of kaolinite. *J. Colloid Interface Sci.* **2001**, *244*, 359–364. [CrossRef]

50. Breen, C.; Illés, J.; Yarwood, J.; Skuse, D.R. Variable temperature diffuse reflectance infrared fourier transform spectroscopic investigation of the effect of ball milling on the water sorbed to kaolin. *Vib. Spectrosc.* **2007**, *43*, 366–379. [CrossRef]

51. Frost, R.L.; Kristof, J.; Paroz, G.N.; Kloprogge, J.T. Role of water in the intercalation of kaolinite with hydrazine. *J. Colloid Interface Sci.* **1998**, *208*, 216–225. [CrossRef]